Journal of Optics

ACCEPTED MANUSCRIPT • OPEN ACCESS

Lattice topological edge and corner modes of photonic crystal slabs

To cite this article before publication: Zhaojian Zhang *et al* 2021 *J. Opt.* in press https://doi.org/10.1088/2040-8986/ac1832

Manuscript version: Accepted Manuscript

Accepted Manuscript is "the version of the article accepted for publication including all changes made as a result of the peer review process, and which may also include the addition to the article by IOP Publishing of a header, an article ID, a cover sheet and/or an 'Accepted Manuscript' watermark, but excluding any other editing, typesetting or other changes made by IOP Publishing and/or its licensors"

This Accepted Manuscript is **© 2021 The Author(s). Published by IOP Publishing Ltd.**.

As the Version of Record of this article is going to be / has been published on a gold open access basis under a CC BY 3.0 licence, this Accepted Manuscript is available for reuse under a CC BY 3.0 licence immediately.

Everyone is permitted to use all or part of the original content in this article, provided that they adhere to all the terms of the licence https://creativecommons.org/licences/by/3.0

Although reasonable endeavours have been taken to obtain all necessary permissions from third parties to include their copyrighted content within this article, their full citation and copyright line may not be present in this Accepted Manuscript version. Before using any content from this article, please refer to the Version of Record on IOPscience once published for full citation and copyright details, as permissions may be required. All third party content is fully copyright protected and is not published on a gold open access basis under a CC BY licence, unless that is specifically stated in the figure caption in the Version of Record.

View the article online for updates and enhancements.

This content was downloaded from IP address 144.82.114.191 on 03/08/2021 at 16:52

Lattice topological edge and corner modes of photonic crystal slabs

Z Zhang[1], J W You[1]‡, Z Lan[1] and N C Panoiu[1]

[1] Department of Electronic and Electrical Engineering, University College London, Torrington Place, London WC1E 7JE, United Kingdom

E-mail: n.panoiu@ucl.ac.uk

22 July 2021

Abstract. Surface lattice modes, generated by the evanescent coupling between localized modes of optical resonators arranged in a two-dimensional (2D) array, generally exhibit remarkable optical response beyond the single photonic particle. Here, by employing the lattice mode concept, we demonstrate that lattice topological edge and corner modes can be achieved in properly designed photonic crystal (PhC) slabs. Such slabs consist of an array of finite-sized second-order topological insulators mimicking the 2D Su-Schrieffer-Heeger model. The proposed lattice edge and corner modes emerge within the topological band gap of the PhC slab, which dictates their topological nature. In particular, the band diagram of the lattice corner modes shows that they possess non-degenerate eigenfrequencies and dispersive bands. In addition, we show that the eigenfrequency of the lattice topological modes can be shifted by tuning the intercell and/or intracell optical coupling. Finally, by finely tuning the geometric parameters of the slab, we realize a lattice corner mode possessing flatband dispersion characteristics. Our study can find applications to topological lasing, nonlinearity enhancement, and slow-light effects in topological photonic systems.

‡ Present address: Southeast University, State Key Laboratory of Millimeter Waves, No. 2 Southeast University Road, Nanjing, 211189, China.

Accepted Manuscript

1. Introduction

Originally discovered in condensed-matter systems [1, 2] and later on extended to photonics [3, 4] and other disciplines, topological insulators (TIs) have recently attracted much attention due to their intriguing bulk-edge properties. For instance, topological photonic systems can support topologically protected edge modes, which are immune to perturbations and backscattering [5, 6, 7, 8], thus providing a robust way to manipulate the flow of light. By now, photonic topological states have been realized in various photonic platforms, such as, PhCs (PhCs) [9, 10], metamaterials [11, 12], and mutually-coupled optical waveguides [13, 14, 15]. In addition to a growing fundamental scientific interest revolving around their unique physical properties, we have recently witnessed the emergence of a variety of promising applications based on photonic topological states, including robust slow light [16, 17, 18], nonlinear enhancement of optical interactions [19, 20, 21, 22], lasing [23, 24, 25], and sensing [26].

Recently, the concept of higher-order topological insulators (HOTIs) has been proposed [27, 28]. Different from conventional TIs, HOTIs possess lower-dimensional topological states, e.g., two-dimensional (2D) second-order TIs (SOTIs) possess 0D corner states. Generally, there are two ways to construct SOTIs. One approach is to realize bulk quadrupole polarization by introducing negative coupling between photonic resonators [29, 30, 31]. This, however, is challenging for compact photonic integration due to compatibility issues. The alternative approach is to use edge dipole polarization described by the 2D Zak phase [28, 32]. So far, SOTIs based on PhCs have been studied both theoretically and experimentally [33, 34, 35], offering appealing opportunities for practical applications, such as high-Q optical cavities and topological lasing with low threshold [36, 37].

Up to now, the studies of photonic SOTIs have mainly focused on the properties of isolated corner modes, meaning that the effect of the coupling among corner modes has not been investigated. It has been known that [38], some limitations of optical resonances of particles, such as the rather small quality(Q)-factor, can be overcome when the resonant particles form periodic arrays, due to the considerable near-field and far-field interactions among them. In the context of photonics, such collective resonances are often referred to as lattice resonances. They can play an important role in photonic systems and lead to novel optical effects, including large field enhancement and resonance narrowing.

In this paper, we introduce the concept of lattice topological edge and corner modes by arranging photonic SOTIs in a periodic array. Each photonic SOTI is designed based on the 2D Su-Schrieffer-Heeger (SSH) model, and serves as a supercell of our PhC slab. In such purposely designed PhC slab, the optically coupled topological edge and corner modes display the features of surface lattice modes, due to the substantial interaction among the SOTI supercells. Here, we focus on the Bloch band properties of these lattice topological edge and corner modes, and reveal that they not only possess non-degenerate eigenfrequencies, but also exhibit dispersive features that can be readily engineered. To gain deeper physical insights into such exotic dispersive features, the influence of intercell and intracell mode coupling on the optical properties lattice corner modes is also investigated. Additionally, we demonstrate that lattice corner modes characterized by flat bands can be created by simply tuning the geometric parameters of the PhC slab. This work introduces the lattice mode concept into the realm of topological photonics, where the resulting outstanding features could be promising for practical applications in areas such as topologically protected lasing, nonlinear field enhancement, and slow light.

The paper is organized as follows. In Sec. 2, the geometrical configuration and material parameters of the proposed PhC slab are presented, whereas in Sec. 3 we describe its band structure and topological properties. Then, in Sec. 4, we introduce the lattice topological edge and corner modes and investigate their optical properties, including their band frequency dispersion, the effect of optical coupling on their physical properties, and the existence of flat-band features. The main conclusions and future prospects are summarized in Sec. 5.

2. Geometrical configuration and material parameters

The geometrical configuration of the dielectric PhC slab proposed as a platform for the implementation of HOTIs that support lattice topological edge and corner modes is presented in Fig. 1. It consists of a periodic arrangement of PhC supercells, each of which being composed of a finite number of square unit cells. The lattice constant of the unit cell and supercell are a and b, respectively. The thickness of the slab is $t = 0.74a$, and the dielectric constant $\varepsilon = 12$. As depicted in Fig. 1, each supercell contains a region filled with nontrivial unit cells, which are surrounded by trivial unit cells, where m denotes the number of trivial unit cells between adjacent nontrivial regions and n the number of nontrivial unit cells within one supercell. Here, the nontrivial (trivial) unit cell refers to the topological nontrivial (trivial) phase that the unit cell possesses. This terminology will be defined and discussed in detail in the next section.

Accepted Manuscript

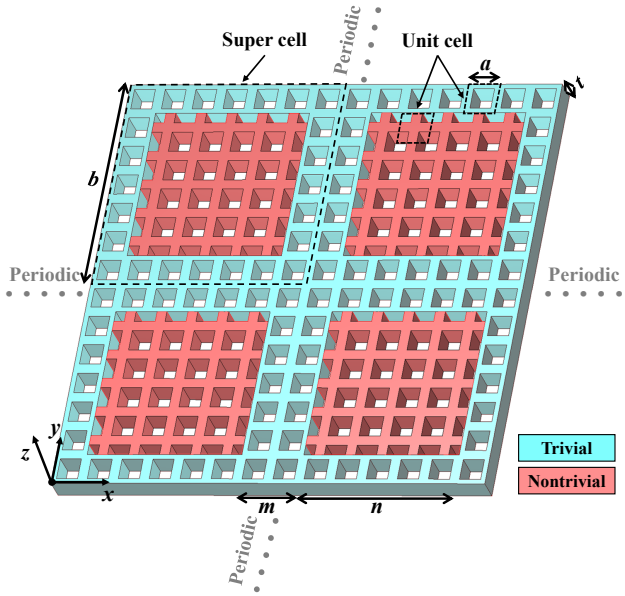

Figure 1. Schematic of a dielectric PhC slab supporting lattice topological edge and corner modes. The PhC slab consists of a periodic array of supercells, which include both trivial and nontrivial unit cells, highlighted in blue and red, respectively.

The parameters n and m allow us to tune the interaction between the optical modes of the supercells. Thus, it can be seen that by varying m the spacing between the nontrivial domains changes and consequently the optical interaction between the edge or corner modes located in adjacent supercells can be modified. On the other hand, by changing n, one can tune the optical interaction between edge and corner modes located inside the same supercell. Therefore, varying the parameters n and m provides a convenient way to tune the intra- and inter-cell optical coupling of edge and corner optical modes and therefore the optical properties of lattice topological modes.

3. Band structure and topological properties

In this section, we present the band structure of the underlying PhC configurations and their topological properties. To begin with, we have employed the plane-wave expansion method implemented in Synopsys's BandSOLVE [39] and computed the photonic band structures of three PhCs with different unit cells. The results of these calculations are summarized in Fig. 2. Note, here we only consider the transverse electric (TE) modes, as in this case one can achieve more readily topological edge and corner modes. All three unit cells contain four identical square air holes with side length $l = 0.34a$, located at different positions inside the unit cell. When the four air holes occupy symmetrically the four quadrants of the unit cell, the corresponding band structure, presented in Fig. 2(a) (only the first

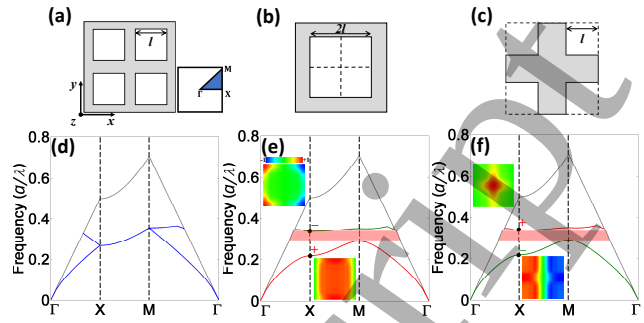

Figure 2. (a)-(c) Schematics of three unit cells. The gray and white areas represent dielectric and air regions, respectively. The FBZ is indicated in (a). (d)-(f) The first two TE bands of the PhC with unit cells in (a)-(c), respectively, where the light line is in gray. In (e) and (f), the light red strips indicate the band gap, and the insets are normalized field distributions of H_z at the X symmetry point. The band colors indicate a band inversion, and symbols $+$ and $-$ indicate even and odd parity of H_z, respectively.

two bands below the light cone are included), shows two bands that are degenerate along the $X-M$ crystal symmetry axis.

When the four air holes are shifted inwardly or outwardly along the $\Gamma - M$ crystal symmetry axis, the band degeneracy is lifted and the photonic system emulates the 2D SSH model [32]. In this model, there are four atoms in each unit cell, and by tuning the intracell (atoms in the same unit cell) and intercell (atoms in different unit cells) hopping amplitudes t_a and t_b, by varying the distance between the atoms, one can induce topological phase transitions. The corresponding topological properties are described by the tight-binding model, whose Hamiltonian is expressed as follows [32]:

$$\mathcal{H}(\mathbf{k}) = \begin{pmatrix} 0 & h_{12} & h_{13} & 0 \\ h_{12}^* & 0 & 0 & h_{24} \\ h_{13}^* & 0 & 0 & h_{34} \\ 0 & h_{24}^* & h_{34}^* & 0 \end{pmatrix}, \quad (1)$$

where $h_{12} = h_{34} = t_a + t_b e^{ik_x}$, $h_{13} = h_{24} = t_a + t_b e^{-ik_y}$, and $\mathbf{k} = (k_x, k_y)$ is the normalized wave vector. In our PhC slab, the four air holes play the role of the four atoms in the unit cell of the SSH model, and moving the centers of the four air holes changes the intracell and intercell optical coupling, which is the analogue of tuning the hopping amplitudes in the SSH model.

As illustrated in Fig. 2(b), if the four air holes move inwards along the diagonal of the unit cell and merge into a single air hole with side length $2l$, a complete band gap is created as indicated by the red strip in Fig. 2(e). Likewise, an identical band gap is created when the four air holes move outwards along the diagonal of the unit cell to the edges of the unit cell, as depicted in Fig. 2(c).

A band inversion between the bands shown in

Accepted Manuscript

Figs. 2(e) and 2(f) can be identified from the parities of the bands. To be more specific, we present the normalized field profile of H_z at the X symmetry point in the insets of Figs. 2(e) and 2(f), determined in the x-y plane crossing through the middle of the PhC slab and perpendicular onto the z-axis. Note, H_z field distributions in the same x-y cross-section are shown in the following section unless stated otherwise. As can be seen from Fig. 2(e), at the X symmetry point the field distribution of H_z corresponding to the first band has even parity, whereas the second band has odd parity. By contrast, the parity of H_z in Fig. 2(f) displays the opposite behavior. Such parity inversion indicates that the two bands have been inverted, a process accompanied by a topological phase transition.

To demonstrate that a topological phase transition occurs when the air holes are displaced along the diagonal of the unit cell, we calculate the 2D Zak phase for the unit cells shown in Figs. 2(b) and 2(c). Here, the unit cell of the PhC slab is simulated in COMSOL [40], where finite-element method (FEM) is utilized to calculate the frequencies and field distributions of the modes. The 2D Zak phase is defined as follows [28]:

$$\theta_\alpha = 2\pi P_\alpha = \frac{1}{2\pi}\int_{\mathrm{FBZ}} \mathrm{Tr}[A_\alpha(\mathbf{k})]d\mathbf{k}, \quad \alpha = x, y, \tag{2}$$

where $\mathbf{P} = (P_x, P_y)$ is the 2D polarization, and $A_\alpha(\mathbf{k}) = i\langle\psi_\mathbf{k}|\partial_{k_\alpha}|\psi_\mathbf{k}\rangle$ is the Berry connection with $|\psi_\mathbf{k}\rangle$ being the eigenmodes of all the bands below the band gap.

Utilizing the 3D eigenmode functions obtained via FEM in COMSOL, we have confirmed that the unit cell in Fig. 2(b) possesses 2D Zak phases $\theta_x = \theta_y = 0$, indicating that it is characterized by a trivial topological phase. By contrast, the Zak phase is $\theta_x = \theta_y = \pi$ for the unit cell in Fig. 2(c), meaning that the corresponding PhC has a nontrivial topological phase. The details about the calculation of the 2D Zak phase are presented in the Appendix.

4. Lattice topological edge and corner modes

So far, most studies of SOTIs have focused on isolated corner modes of a finite photonic structure containing nontrivial unit cells and surrounded by trivial unit cells [28]. Here, we arrange SOTIs so as the system is periodic along x- and y-axis, which means that each SOTI represents a supercell in the PhC slab shown in Fig. 1.

For the case characterized by $m = 1$ and $n = 5$, we give in Fig. 3(a) the eigenmode frequencies of the PhC slab determined at the Γ symmetry point. There are four topological edge modes and four topological corner modes inside the band gap, and the corresponding field distributions of the H_z component, determined in the $x - y$ plane of the supercell at $z = 0$, are presented in Figs. 3(b) and 3(c). These plots show that the field of the edge modes is distributed at the two edges of the supercell, whereas the field of the corner modes is primarily localized at the four corners of the supercell.

It is worth to note that the four corner modes plotted here, namely quadrupole (q), dipole 1 (d_1), dipole 2 (d_2), and monopole (m) modes [37], have non-degenerate eigenfrequencies, a feature that differentiates them from the conventional corner modes of an isolated SOTI. This difference is mainly due to the interaction among the optical fields in different supercells, namely, due to the intercell and intracell optical coupling of the corner modes.

In order to study the influence of intercell optical coupling on the physical properties of the lattice topological edge and corner modes, we fix $n = 5$ and increase m from $m = 1$ to $m = 2$. The frequencies and field profiles of the new set of optical modes are presented in Fig. 4(a). These results suggest that both

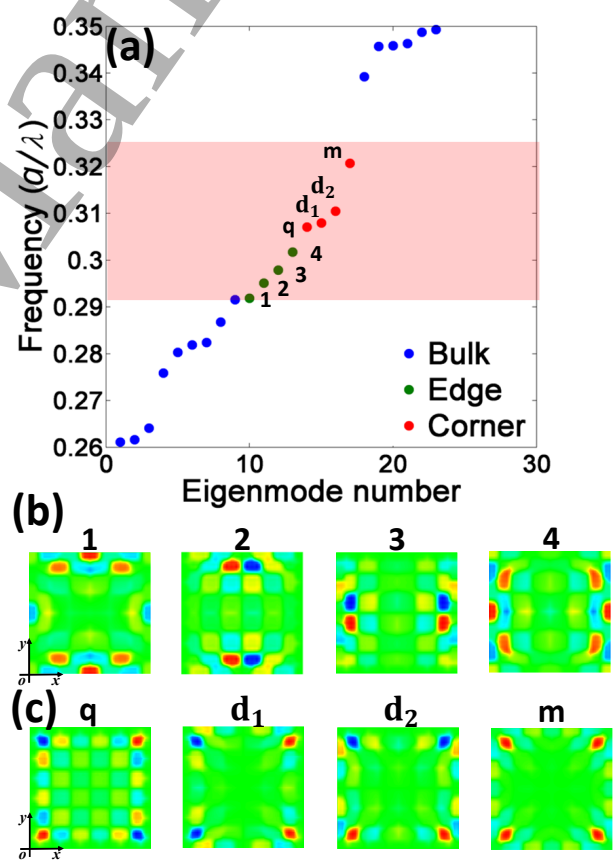

Figure 3. (a) The eigenmodes of the PhC slab with supercell shown in Fig. 1, determined at the Γ symmetry point for $m = 1$, $n = 5$, where bulk, edge, and corner modes are represented in blue, green, and red, respectively and the light-red regions indicate the band gap. Edge modes are numbered and corner modes are labeled as explained in the text. (b), (c) Normalized field distributions H_z for the edge and corner modes in (a), respectively, determined in the $x - y$ plane at $z = 0$.

Accepted Manuscript

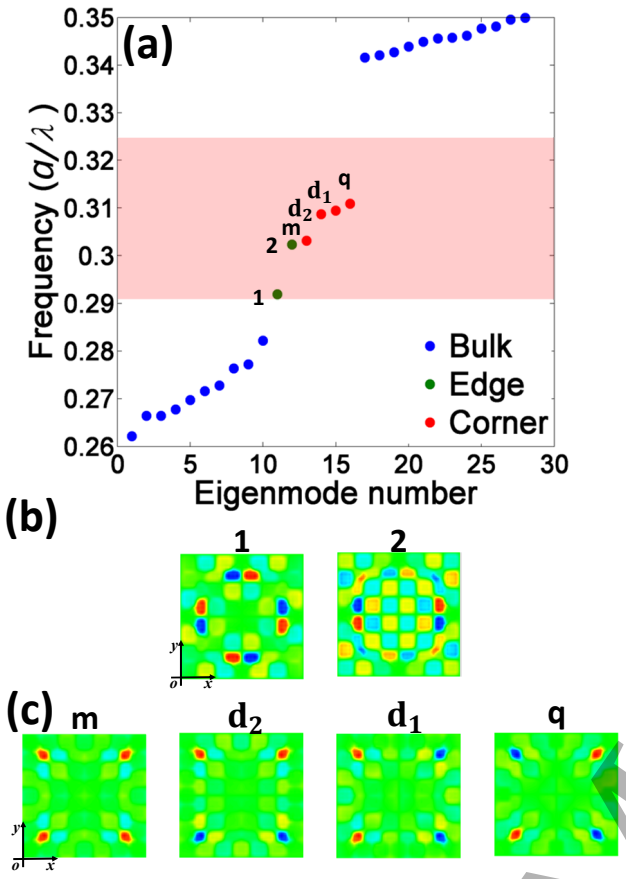

Figure 4. (a) The eigenmodes of the PhC slab with supercell shown in Fig. 1, determined at the Γ symmetry point for $m = 2$, $n = 5$. (b), (c) Normalized field distributions H_z for the edge and corner modes in (a), respectively, determined in the $x - y$ plane at $z = 0$.

the eigenmode frequencies and the corresponding field profiles, determined at the Γ symmetry point, vary markedly when adding just one row of unit cells to the SOTI supercell, cf. Fig. 3(a). Specifically, as each supercell becomes larger, the number of bulk modes increases. In addition, as a result of the evanescent nature of the optical coupling, the mode interaction in this case is weaker and two of the four edge modes are pulled into the bulk region. Furthermore, the frequencies of the four corner modes are shifted and, interestingly enough, their order changes, too. These findings indicate that the frequency dispersion of the topological edge and corner modes can be controlled by properly engineering their intercell optical interaction. Since this is a feature similar to that of surface lattice modes of plasmonic metasurfaces [38], we call these extended modes located within the band gap of the PhC slab *lattice topological edge and corner modes*.

4.1. Band dispersion of lattice topological edge and corner modes

In an isolated SOTI, the edge modes are generally dispersive, but the corner modes are non-dispersive and usually degenerate [28]. Different from the edge and corner modes of an isolated SOTI, the lattice topological edge and corner modes introduced in this work can display strong frequency dispersion, which is an important physical property especially from a practical point of view. To further illustrate this idea, the band structures of the lattice edge and corner modes of the PhC slab depicted in Fig. 1 with $m = 1$ and $n = 5$, obtained when varying k_x, are presented in Figs. 5(a) and 5(b), respectively.

The mode dispersion curves presented in Fig. 5(a) show that the bands are symmetric with respect to $k_x = 0$, in contrast with the case of topological photonic systems that do not possess time-reversal symmetry. In addition, one can see that the sign of the group-velocity, v_g, of the edge bands 1 and 2 is opposite as compared to that of the edge bands 3 and 4. This same property is true for the v_g of the q and m corner bands on the one hand and the dipole corner bands on the other hand. This is explained by the fact that the corresponding bands have opposite convexity. More notably, different from the degenerate and non-dispersive nature of the corner modes of an isolated SOTI, the four bands of the lattice topological corner modes show non-degenerate and dispersive behavior upon the variation of k_x, as illustrated in Fig. 5(b).

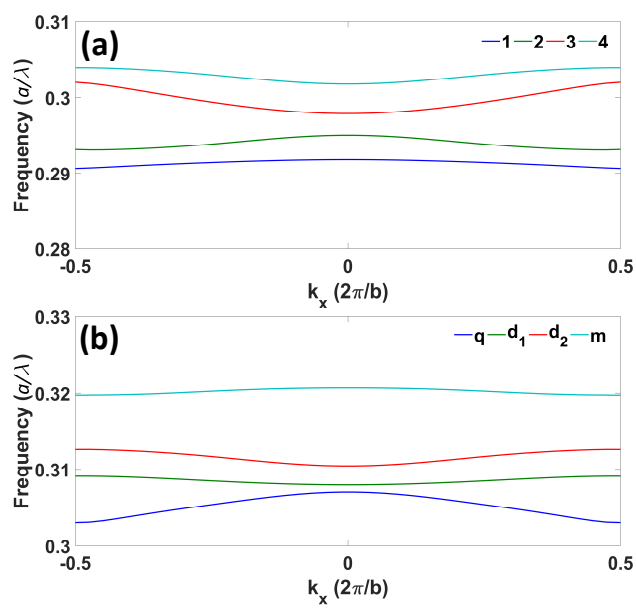

Figure 5. Mode dispersion of (a) lattice topological edge modes and (b) lattice topological corner modes of the PhC slab shown in Fig. 1 and characterized by $m = 1$ and $n = 5$.

Accepted Manuscript

4.2. Intercell and intracell coupling effect on lattice corner modes

To gain deeper physical insights into the dispersion properties of the lattice corner modes, the influence of intercell and intracell optical coupling effects on their properties is further investigated in this subsection. As we just demonstrated, the strength of the intercell coupling can be readily tuned by changing the number of rows of trivial PhC material surrounding the topological nontrivial region, m. As shown in Fig. 6(a), the frequencies of the four lattice corner modes converge asymptotically to a common value when one increases the value of m while keeping n fixed ($n = 5$ in this case). This phenomenon indicates that the lattice corner bands would become degenerate, as it is the case with the corner modes of an isolated SOTI, if the optical interaction among the supercells vanishes. Conversely, the degeneracy of the corner modes is lifted when one decreases m, because smaller m leads to larger intercell optical coupling among the supercells.

In addition to the intercell optical coupling effects just discussed, the intracell coupling, namely the mutual interaction of the four corner modes located within the same supercell, can also play an important role in determining the dispersion properties of the lattice corner modes. To study the influence of the intracell optical coupling on the lattice corner modes, we vary the value of n but fix the parameter m to $m = 5$. As presented in Fig. 6(b), the spread between the frequencies of the four lattice corner modes increases as n decreases, which again illustrates the evanescent nature of the optical coupling among the corner modes.

4.3. Flatbands originating from lattice corner modes

Recently, chiefly due to their intriguing physical properties and applications, photonic flatbands are drawing increasing attention in both theory and experiments [41]. As an analogue of states observed in condensed matter systems, such dispersionless bands possess not only fundamental research significance but also potential applications to quantum simulation systems [42] and platforms for implementation of slow-light based applications [43]. To date, photonic flatbands have been realized in various photonic systems, such as waveguide arrays [44, 45], exciton-polariton systems [46, 47], and metasurfaces [48, 49].

Here, since the band dispersion of dipole 1 mode is relatively weak, as per Fig. 5(b), we aim to flatten this band by finely tuning the geometric parameters l and t of the PhC slab, namely the side length of the square air hole and the thickness of the PhC slab, respectively. As shown in Fig. 7, where the band dispersion corresponding to the four corner lattice modes is depicted, a flatband associated to the dipole 1 mode can be achieved, when the geometry parameters are chosen as $l = 0.39a$ and $t = 0.65a$. We emphasize that as the other three bands remain dispersive, the emergence of this flat band is not due to some trivial phenomena, such as lack of intercell mode interaction, as that would result in the creation of four flat bands. In addition, flatbands designed by such fine-tuning can be classified as accidental flatbands [41].

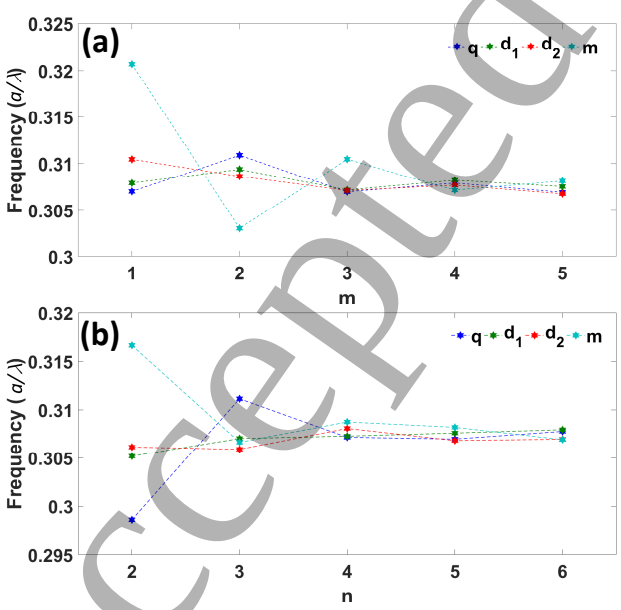

Figure 6. Dependence of the frequencies of lattice corner modes, determined at the Γ symmetry point, on (a) m when $n = 5$ and (b) n when $m = 5$.

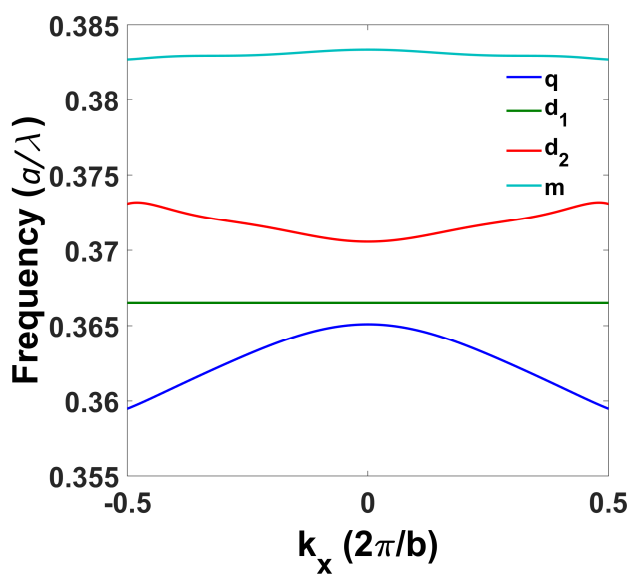

Figure 7. Band structure of the lattice corner modes, determined for $l = 0.39a$ and $t = 0.65a$. In this case, the band of dipole 1 is flat while the other three bands are dispersive.

Accepted Manuscript

5. Conclusion

In conclusion, we have proposed a specially designed PhC slab composed of periodically arranged SOTIs based on the 2D SSH model, which supports lattice topological edge and corner modes. We have found that the lattice corner modes possess non-degenerate eigenfrequencies and form dispersive bands, a feature distinct from the widely studied degenerate corner modes in individual SOTIs. We have further investigated the influence of intercell and intracell optical coupling on the lattice edge and corner modes, and demonstrated that a flatband corresponding to a lattice corner mode can be readily realized by tuning the configuration of the topological PhC slab.

In general, the corner modes of individual SOTI possess a large quality factor, thus the lattice corner modes proposed in this work may as well inherit this property. Consequently, the transmittance and reflectance spectra of the PhC slab structures proposed in this work could become a promising platform for implementation of topologically protected lasing, nonlinear enhancement of optical interactions, sensing, and other nanophotonic applications. Moreover, the feasibility to design photonic flatbands using lattice corner modes could make the proposed PhC slab suitable for flatband related applications, such as quantum simulation and active devices based on slow-light effects.

Appendix

The 2D Zak phase is introduced by analogy with its definition in the 1D case [50]:

$$\theta = \int_{-\pi}^{\pi} A_n(k)dk. \tag{3}$$

Here, $A_n(k) = i\langle u_n(k)|\partial_k|u_n(k)\rangle$ is the Berry connection, where $|u_n(k)\rangle$ is the periodic Bloch function and n runs over all the bands below the band gap. Since in our case there is only one band below the band gap, n will be omitted in the following discussion. Note, the integration in the equation above is over the 1D FBZ, and the lattice constant a is set to unity to simplify the presentation [51].

In our calculations, the 1D FBZ is divided into N segments, and the discrete Zak phase in a small segment connecting k_α and $k_{\alpha+1}$ is $\theta_\alpha = A(k_\alpha)\Delta k = i\langle u(k_\alpha)|u(k_{\alpha+1})\rangle - i$. Therefore one can infer that,

$$\langle u(k_\alpha)|u(k_{\alpha+1})\rangle = 1 - i\theta_\alpha \approx e^{-i\theta_\alpha}, \quad \alpha = 1, \ldots, N. \tag{4}$$

Based on the Wilson-loop approach, the total Zak phase can be calculated by compounding the discrete Zak phase from each small segment as follows:

$$e^{-i\theta} = \prod_{\alpha=1}^{N} e^{-i\theta_\alpha} = \prod_{\alpha=1}^{N} \langle u(k_\alpha)|u(k_{\alpha+1})\rangle. \tag{5}$$

Therefore, the total Zak phase can be expressed as:

$$\theta = -\mathfrak{Im}\left[\ln\left(\prod_{\alpha=1}^{N} \langle u(k_\alpha)|u(k_{\alpha+1})\rangle\right)\right]. \tag{6}$$

When the Zak phase is extended to 2D, namely, (k_x, k_y) in the 2D FBZ, the x-component of the 2D Zak phase, for example, can be written as follows:

$$\theta_x(k_y) = -\mathfrak{Im}\left[\ln\left(\prod_{\alpha=1}^{N} \langle u(k_\alpha, k_y)|u(k_{\alpha+1}, k_y)\rangle\right)\right]. \tag{7}$$

Here, along each axis the 2D FBZ is partitioned in the same way as described above in the case of 1D FBZ. Therefore, the total 2D Zak phase associated to the k_x-axis is given by:

$$\theta_x = \frac{1}{2\pi}\int_{-\pi}^{\pi} \theta_x(k_y)dk_y, \tag{8}$$

whereas the corresponding k_y-component is calculated in the same manner.

In this paper, all the calculations are based on the 3D PhC slab. Therefore, the scalar product $\langle u(\mathbf{k})|u(\mathbf{k}')\rangle$ is calculated as follows:

$$\langle u(\mathbf{k})|u(\mathbf{k}')\rangle = \int \varepsilon(\mathbf{r})u^*(\mathbf{r};\mathbf{k})u(\mathbf{r};\mathbf{k}')d\mathbf{r}. \tag{9}$$

We have calculated the 2D Zak phase for both the unit cells in Figs. 2(b) and 2(c). For example, for the unit cell in Fig. 2(b), the corresponding θ_x (θ_y) is zero for all values of k_y (k_x). Moreover, following Eq. (8), we can determine that the total 2D Zak phase is (0, 0), indicating that such unit cell corresponds to a trivial topological phase. Similarly, we can also confirm that the unit cell in Fig. 2(c) possesses 2D Zak phase equal to (π, π), meaning that the unit cell in this case has a nontrivial topological phase.

Funding

European Research Council (ERC-2014-CoG-648328); China Scholarship Council; University College London.

Disclosures

The authors declare no conflicts of interest.

5.1. References

[1] Hasan M Z and Kane C L 2010 Colloquium: Topological insulators *Rev. Mod. Phys.* **82** 3045–67.
[2] Qi X L and Zhang S C 2011 Topological insulators and superconductors *Rev. Mod. Phys.* **83** 1057–1110.
[3] Lu L, Joannopoulos J D, and Soljačić M 2014 Topological photonics *Nat. Photonics* **8** 821–829.
[4] Ozawa T, Price H M, Amo A, Goldman N, Hafezi M, Lu L, Rechtsman M C, Schuster D, Simon J, Zilberberg O, and Carusotto I 2019 Topological photonics *Rev. Mod. Phys.* **91** 015006.

Accepted Manuscript

[5] Wang Z, Chong Y, Joannopoulos J D, and Soljacic M 2008 Reflection-free one-way edge modes in a gyromagnetic PhC *Phys. Rev. Lett.* **100** 013905.

[6] Noh J, Huang S, Chen K P, and Rechtsman M C 2018 Observation of photonic topological valley Hall edge states *Phys. Rev. Lett.* **120** 063902.

[7] He X T, E. T. Liang E T, Yuan J J, Qiu H Y, Chen X D, Zhao F L, and Dong J W 2019 A silicon-on-insulator slab for topological valley transport *Nat. Commun.* **10** 872.

[8] Shalaev M I, Walasik W, Xu A, Tsukernik Y, and Litchinitser N M 2019 Robust topologically protected transport in PhCs at telecommunication wavelengths *Nat. Nanotechnol.* **14** 31–34.

[9] Wu L H and Hu X 2015 Scheme for achieving a topological PhC by using dielectric material *Phys. Rev. Lett.* **114** 223901.

[10] Lu L, Fang C, Fu L, Johnson S G, Joannopoulos J D, and Soljačić M 2016 Symmetry-protected topological PhC in three dimensions *Nat. Phys.* **12** 337–340.

[11] Khanikaev A B, Hossein Mousavi S, Tse W K, Kargarian M, MacDonald A H, and Shvets G 2013 Photonic topological insulators *Nat. Mater.* **12** 233–239.

[12] Guo Q, Yang B, Xia L, Gao W, Liu H, Chen J, Xiang Y, and Zhang S 2017 Three Dimensional Photonic Dirac Points in Metamaterials *Phys. Rev. Lett.* **119** 213901.

[13] Cheng Q, Pan Y, Wang Q, Li T, and Zhu S 2015 Topologically protected interface mode in plasmonic waveguide arrays *Laser Photonics Rev.* **9** 392–398.

[14] Noh J, Benalcazar W A, Huang S, Collins M J, Chen K P, Hughes T L, and Rechtsman M C 2018 Topological protection of photonic mid-gap defect modes *Nat. Photonics* **12** 408-415.

[15] You J W, Lan Z, Bao Q, and Panoiu N C 2020 Valley-Hall topological plasmons in a graphene nanohole plasmonic crystal waveguide *IEEE J. Sel. Top. Quantum Electron* **26** 4600308.

[16] Hafezi M, Demler E A, Lukin M D, and Taylor J M 2011 Robust optical delay lines with topological protection *Nat. Phys.* **7** 907–912.

[17] Gangaraj S A H and Monticone F 2018 Topological waveguiding near an exceptional point: defect-immune, slow-light, and loss-immune propagation *Phys. Rev. Lett.* **121** 093901.

[18] Yoshimi H, Yamaguchi T, Ota Y, Arakawa Y, and Iwamoto S 2020 Slow light waveguides in topological valley PhCs *Opt. Lett.* **45** 2648-2651.

[19] Smirnova D, Kruk S, Leykam D, Melik-Gaykazyan E, Choi D Y, and Kivshar Y 2019 Third-harmonic generation in photonic topological metasurfaces *Phys. Rev. Lett.* **123** 103901.

[20] You J W, Lan Z, and Panoiu N C 2020 Four-wave mixing of topological edge plasmons in graphene metasurfaces *Sci. Adv.* **6** eaaz3910.

[21] Lan Z, You J W, and Panoiu N C 2020 Nonlinear one-way edge-mode interactions for frequency mixing in topological PhCs *Phys. Rev. B* **101** 155422.

[22] Lan Z, You J W, Ren Q, Sha W E I, and Panoiu N C 2021 Second-harmonic generation via double topological valley-Hall kink modes in all-dielectric PhCs *Phys. Rev. A* **103** 041502.

[23] Pilozzi L and Conti C 2016 Topological lasing in resonant photonic structures *Phys. Rev. B* **93** 195317.

[24] Bandres M A, Wittek S, Harari G, Parto M, Ren J, Segev M, Christodoulides D N, and Khajavikhan M 2018 Topological insulator laser: Experiments *Science* **359** 6381.

[25] Zeng Y, Chattopadhyay U, Zhu B, Qiang B, Li J, Jin Y, Li L, Davies A G, Linfield E H, Zhang B, Chong Y, and Wang Q J 2020 Electrically pumped topological laser with valley edge modes *Nature* **578** 246-250.

[26] Wang Y, You J W, Lan Z, and Panoiu N C 2020 Topological valley plasmon transport in bilayer graphene metasurfaces for sensing applications *Opt. Lett.* **45** 3151-3154.

[27] Benalcazar W A, Bernevig B A, and Hughes T L 2017 Quantized electric multipole insulators *Science* **357** 61-66.

[28] Xie B Y, Wang H F, Wang H X, Zhu X Y, Jiang J H, Lu M H, and Chen Y F 2018 Second-order photonic topological insulator with corner states *Phys. Rev. B* **98** 205147.

[29] Peterson C W, Benalcazar W A, Hughes T L, and Bahl G 2018 A quantized microwave quadrupole insulator with topologically protected corner states *Nature* **555** 346-350.

[30] Serra-Garcia M, Peri V, Süsstrunk R, Bilal O R, Larsen T, Villanueva L G, and Huber S D 2018 Observation of a phononic quadrupole topological insulator *Nature* **555** 342-345.

[31] Mittal S, Orre V V, Zhu G, Gorlach M A, Poddubny A, and Hafezi M 2019 Photonic quadrupole topological phases *Nat. Photonics* **13** 692-696.

[32] Liu F and Wakabayashi K 2017 Novel topological phase with a zero berry curvature *Phys. Rev. Lett.* **118** 076803.

[33] Xie B Y, Su G X, Wang H F, Su H, Shen X P, Zhan P, Lu M H, Wang Z L, and Chen Y F 2019 Visualization of higher-order topological insulating phases in 2D dielectric PhCs *Phys. Rev. Lett.* **122** 233903.

[34] Chen X D, Deng W M, Shi F L, Zhao F L, Chen M, and Dong J W 2019 Direct observation of corner states in second-order topological PhC slabs *Phys. Rev. Lett.* **122** 233902.

[35] Ota Y, Liu F, Katsumi R, Watanabe K, Wakabayashi K, Arakawa Y, and Iwamoto S 2019 PhC nanocavity based on a topological corner state *Optica* **6** 786-789.

[36] Zhang W, Xie X, Hao H, Dang J, Xiao S, Shi S, Ni H, Niu Z, Wang C, Jin K, Zhang X, and Xu X 2020 Low-threshold topological nanolasers based on the second-order corner state *Light. Sci. Appl.* **9** 1-6.

[37] Kim H R, Hwang M S, Smirnova D, Jeong K Y, Kivshar Y, and Park H G 2020 Multipolar lasing modes from topological corner states *Nat. Commun.* **11** 1-8.

[38] Kravets V G, Kabashin A V, Barnes W L, and Grigorenko A N 2018 Plasmonic surface lattice resonances: a review of properties and applications *Chem. Rev.* **118** 5912-5951.

[39] BandSOLVE, https://www.synopsys.com

[40] COMSOL Multiphysics, https://uk.comsol.com

[41] Leykam D and Flach S 2018 Perspective: photonic flatbands *APL Photonics* **3** 070901.

[42] Vicencio R A, Cantillano C, Morales-Inostroza L, Real B, Mejía-Cortés C, Weimann S, Szameit A, and Molina M I 2015 Observation of localized states in Lieb photonic lattices *Phys. Rev. Lett.* **114** 245503.

[43] Li J, White T P, O'Faolain L, Gomez-Iglesias A, and Krauss T F 2008 Systematic design of flat band slow light in PhC waveguides *Opt. Express* **16** 6227-6232.

[44] Guzmán-Silva D, Mejía-Cortés C, Bandres M, Rechtsman M, Weimann S, Nolte S, Segev M, Szameit A, and Vicencio R 2014 Experimental observation of bulk and edge transport in photonic Lieb lattices *New J. Phys.* **16** 063061.

[45] Mukherjee S, Spracklen A, Choudhury D, Goldman N, Öhberg P, Andersson E, and Thomson R R 2015 Observation of a localized flat-band state in a photonic Lieb lattice *Phys. Rev. Lett.* **114** 245504.

[46] Baboux F, Ge L, Jacqmin T, Biondi M, Galopin E, Lemaître A, Le Gratiet L, Sagnes I, Schmidt S, Türeci H, Amo A, and Bloch J 2016 Bosonic condensation and disorder-induced localization in a flat band *Phys. Rev. Lett.* **116** 066402.

[47] Klembt S, Harder T H, Egorov O A, Winkler K, Suchomel

Accepted Manuscript

H, Beierlein J, Emmerling M, Schneider C, and Höfling S 2017 Polariton condensation in S-and P-flatbands in a 2D Lieb lattice *Appl. Phys. Lett.* **111** 231102.

[48] Kajiwara S, Urade Y, Nakata Y, Nakanishi T, and Kitano M 2016 Observation of a nonradiative flat band for spoof surface plasmons in a metallic Lieb lattice *Phys. Rev. B* **93** 075126.

[49] Moitra P, Yang Y, Anderson Z, Kravchenko I I, Briggs D P, and Valentine J 2013 Realization of an all-dielectric zero-index optical metamaterial *Nat. Photonics* **7** 791-795.

[50] Zak J 1989 Berry's phase for energy bands in solids *Phys. Rev. Lett.* **62** 2747.

[51] Wang H X, Guo G Y, and Jiang J H 2019 Band topology in classical waves: Wilson-loop approach to topological numbers and fragile topology *New J. Phys.* **21** 093029.

Accepted Manuscript